

Reversible lateral optical force on phase-gradient metasurfaces for full control of metavehicles

TIANYUE LI,¹  JACK J. KINGSLEY-SMITH,²  YANHUI HU,²  XIAOHAO XU,^{3,4,7}  SHAOHUI YAN,^{3,5}  SHUMING WANG,^{1,6,8}  BAOLI YAO,^{3,5}  ZHENLIN WANG,¹ AND SHINING ZHU^{1,6}

¹National Laboratory of Solid-State Microstructures, Collaborative Innovation Center for Advanced Microstructures, School of Physics, Nanjing University, Nanjing, 210093, China

²Department of Physics and London Centre for Nanotechnology, King's College London, London WC2R 2LS, UK

³State Key Laboratory of Transient Optics and Photonics Xi'an Institute of Optics and Precision Mechanics (XIOPM), Chinese Academy of Sciences (CAS), Xi'an 710119, China

⁴Institute of Nanophotonics, Jinan University, Guangzhou 511443, China

⁵University of Chinese Academy of Sciences, Beijing 100049, China

⁶Key Laboratory of Intelligent Optical Sensing and Manipulation, Ministry of Education, Nanjing 210093, China

⁷e-mail: xuxhao_dakuren@163.com

⁸e-mail: wangshuming@nju.edu.cn

Received 23 October 2022; revised 2 December 2022; accepted 2 December 2022; posted 2 December 2022; published 2 January 2023

Photonics is currently undergoing an era of miniaturization thanks in part to two-dimensional (2D) optical metasurfaces. Their ability to sculpt and redirect optical momentum can give rise to an optical force, which acts orthogonally to the direction of light propagation. Powered by a single unfocused light beam, these lateral optical forces (LOFs) can be used to drive advanced metavehicles and are controlled via the incident beam's polarization. However, the full control of a metavehicle on a 2D plane (i.e. forward, backward, left, and right) with a sign-switchable LOF remains a challenge. Here we present a phase-gradient metasurface route for achieving such full control while also increasing efficiency. The proposed metasurface is able to deflect a normally incident plane wave in a traverse direction by modulating the plane wave's polarization, and results in a sign-switchable recoil LOF. When applied to a metavehicle, this LOF enables a level of motion control that was previously unobtainable.

© 2023 Optica Publishing Group

<https://doi.org/10.1364/OL.478979>

The momentum exchange between light and matter gives rise to optical forces that can be used to control the motion of objects [1,2]. This ability of light to conduct noncontact manipulation has had a huge impact on the fields of biophotonics [3], quantum physics, and metrology [4,5]. For many years, optical micromanipulation was based on focused or structured light fields, which are generated with bulky optical devices, such as objectives and spatial light modulators [6–8]. However, the recently emerged field of metasurfaces [9–14] has started to facilitate a revolution in this area. Metasurfaces offer an on-chip solution to optical micromanipulation systems by replacing traditional three-dimensional devices with flat, ultrathin optical components [15–20]. More importantly, these artificial materials hold

remarkable performance in deflecting and modifying electromagnetic characteristics, opening the opportunity for the deterministic micromanipulation of simple unfocused light beams.

Metavehicles are maneuverable microstructures launched by an integrated metasurface [21], which reconfigures the momentum of light in order to produce a lateral optical force (LOF) [22–31]. LOFs are at the center of proposed future technologies, including all-optical enantiomer separation [32–35], chip-based optical transport [36], and bottom-up nanofabrication [37]. The LOF caused by a metasurface on a metavehicle is able to control the LOF direction simply by changing the polarization of the incident plane wave, thus enabling the metavehicle to drive in a straight line or turn corners on demand. However, conventional metavehicles [21] are powered and steered by an optical grating metasurface (OGM), which does not allow them to function like everyday vehicles, capable of driving backward. To overcome this drawback, microdrones are designed based on gold nanoantennas, but two light beams of different wavelengths are required to actuate them. In this contribution, we present a fully functional metavehicle based on a phase-gradient metasurface (PGM) that can be actuated in a bidirectional manner, namely, to move both forward and backward (Fig. 1). The ability to steer is provided by elliptical polarization, matching the property of OGM-based metavehicles.

In our study, we consider an input plane wave at normal incidence, propagating in the positive z direction [Fig. 1(a)]. The x axis is aligned to the major axis of the metasurface, which is immersed in water. We define the $+x$ direction as the forward direction. Our first aim is to achieve a LOF on the metasurface pointing in the x direction, with its sign determined by the polarization direction of the input field. To this end, the structure of the metasurface should be symmetrical about its long axis, such that the y component of the LOF can be eliminated by symmetry. Conversely, an anisotropic nanostructure can act as a birefringent truncated waveguide, allowing for the

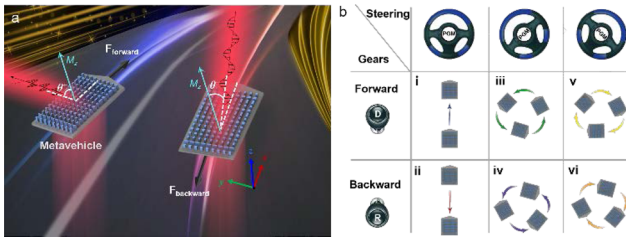


Fig. 1. (a) PGM-based metavehicles, which run forward and backward with different linear polarization scattering; θ^+ and θ^- denote transmission angles at x and y polarization incidence, respectively. (b) Different driving modes available to our metavehicle design, and their analogies to real-world vehicle controls.

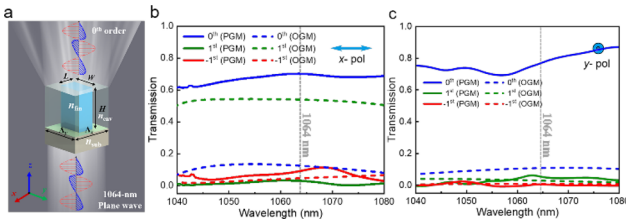


Fig. 2. (a) Metasurface unit cell composed of a-Si nanofins with period $\Lambda_x = \Lambda_y = 520$ nm, fixed height H , and varying length L and width W . (b), (c) Simulated diffraction of two typical unit cells for orders 0 and ± 1 with x and y polarization incidence.

control of the beam deflection. Each unit cell of the PGM is built to exhibit a polarization-dependent optical response, which is the main technical advantage of a PGM over an OGM [11,12,18,19]. Therefore, one may anticipate that the recoiling mechanical effect could be radically different at x and y polarization excitation, respectively.

In principle, the input and output waves are linked by the Jones matrix description: $|E_{out}\rangle = J|E_{in}\rangle$. Such an anisotropic and unitary Jones matrix can be written as [11,18,19]

$$J(x, y) = e^{i\phi^+(x,y)}|q^+\rangle\langle q^-| + e^{i\phi^-(x,y)}|(\bar{q}^+)^*\rangle\langle(\bar{q}^-)^*|, \quad (1)$$

where $\langle q^-|$ is defined as the incident polarization state for which the metasurface will preferentially scatter the directional beam while extinguishing the orthogonal polarization state $\langle(\bar{q}^-)^*|$, and the vector ket $|q^+\rangle$ denotes the polarization state emitted by the interface. Conventionally, the output polarization $|q^+\rangle$ is consistent with incident polarization $\langle q^-|$. In this case, we set $\langle q^-| = [1 \ 0]^T$ with maximum intensity when x polarization is incident, while the response of the other polarizations is low. By changing the incident polarization, the conjugate operator $\langle(\bar{q}^-)^*| = [0 \ 1]^T$ acting on the metasurface will emit y polarization with the other phase profile, while suppressing the x polarization, which conforms to Malus's law [12].

Figure 2(a) shows a typical unit cell with our anisotropic design, composed of amorphous silicon (a-Si, refractive index: $n_{Si} = 3.5$) grown on a fused SiO_2 ($n_{\text{SiO}_2} = 1.45$) substrate in water ($n_{\text{env}} = 1.33$), which can be regarded as a truncated waveguide. Based on Bragg's theorem, the highest efficiency of zeroth order diffraction should fulfill $2\pi/\Lambda_{x,y} < 2\pi n_{\text{sub}}/\lambda$. Here, the lattice constants are set as $\Lambda_x = \Lambda_y = 520$ nm to suppress high-order diffraction, and the height is fixed as $H = 800$ nm. We apply periodic boundary conditions along the x and y axes, set the z axis interfaces to perfectly matched layers and use finite-difference

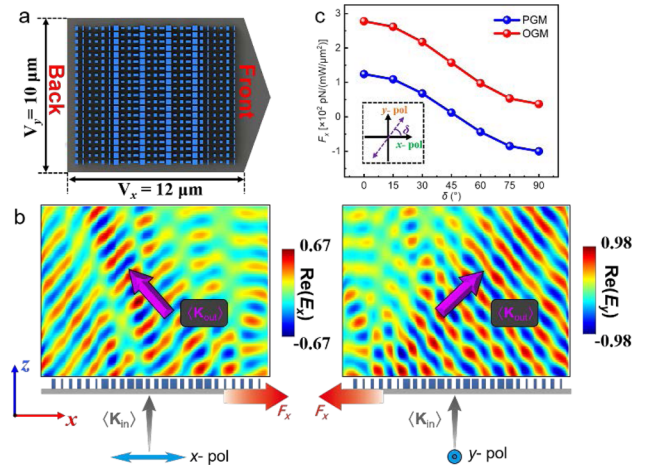


Fig. 3. (a) Configuration of implemented metavehicle. (b) Example of simulated field with orthogonal linear polarization (LP) incidence. (c) LOF on PGM and OGM as a function of polarization angle δ .

time domain (FDTD) simulations to evaluate the optical behavior of the metasurface. The parameters of picked nanopillars for metavehicle design are given in Note 1 of Supplement 1. In particular, we provide a comparison of zeroth and ± 1 st order transmittance for nanocells of PGM and OGM [Figs. 2(b) and 2(c)], respectively, suggesting that the dual-channel PGM not only improves the efficiency of the zeroth order with input y and x polarization, but also further inhibits higher-order diffraction.

According to the previous discussion, a completely operational metavehicle requires both phase gradients in the x direction and periodicity in the y axis. Therefore, ϕ^+ and ϕ^- from Eq. (1) should follow

$$\phi^+(\lambda_0, x) = \frac{2\pi}{\lambda_0} x \sin \theta_i^+ \quad \text{and} \quad \phi^-(\lambda_0, x) = \frac{2\pi}{\lambda_0} x \sin \theta_i^-, \quad (2)$$

where $\theta_i^+ = -\theta_i^- = 45^\circ$ is set for x and y polarization illumination, respectively.

Figure 3(a) shows the layout of the developed PGM, featuring an aperiodic arrangement of nanofins along the x direction. The overall size is in accordance with that of the OGM in Ref. [21]: $12 \mu\text{m} \times 10 \mu\text{m} \times 1 \mu\text{m}$, which can be used for the delivery of unicellular organisms. Figure 3(b) shows the output fields for x and y polarization. While the input plane wave propagates in the z direction, the output field in both cases acquires a transverse component of the wave vector (and therefore momentum), because it varies along a tilted direction. Such a deflection of the propagation direction will yield a recoiling LOF on the PGM, which points in the x direction. According to the momentum conservation law, this recoil force can be expressed as $F_x \propto \langle \mathbf{k}_{in} \rangle_x - \langle \mathbf{k}_{out} \rangle_x = -\langle \mathbf{k}_{out} \rangle_x$, where $\langle \mathbf{k}_{in} \rangle_x$ and $\langle \mathbf{k}_{out} \rangle_x$ are the projections of input and output mean wave vectors on the x axis, such that $\langle \mathbf{k}_{in} \rangle_x = 0$ for normal incidence. Therefore, the PGM will experience a positive LOF under x polarization excitation, and the LOF is expected to change sign for y polarization.

To quantitatively evaluate the LOF, the time-averaged optical force was calculated using the real part of the complex Maxwell stress tensor theorem [38–40]:

$$\mathbf{F} = \oint \vec{\mathbf{T}} \cdot \hat{\mathbf{n}} \, d\sigma, \quad (3)$$

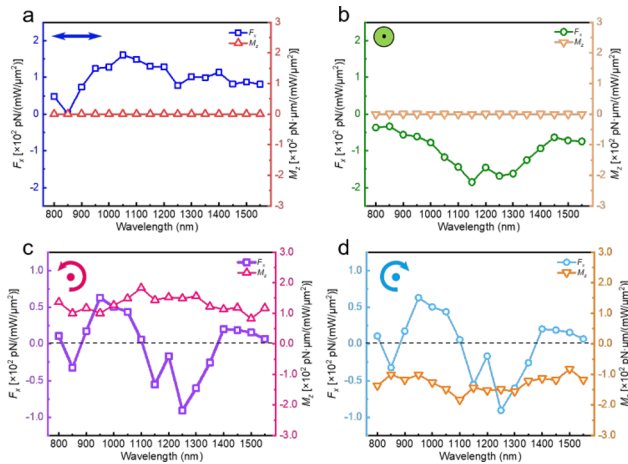


Fig. 4. Broadband results for two classical metasurfaces: (a), (b) force and torque for x and y polarization; (c), (d) results for LCP and RCP illumination.

where $\bar{\mathbf{T}}$ represents the time-averaged Maxwell stress tensor, and \mathbf{n} denotes the unit vector outward and normal to the arbitrary surface σ enclosing the vehicle. We note that the metasurface was originally designed to control the deflection of the transmitted light, but any reflected light may also gain a transverse propagation component and thus contribute to the LOF. However, the Maxwell stress tensor takes this into account by incorporating the total fields around the metasurface.

Figure 3(c) shows the calculated LOF for different input polarization angles with respect to the x axis. Results are shown for both the PGM and OGM, for comparison. We observe that the sign of the LOF on the PGM is switchable with the polarization angle. The sign change occurs near $\delta = 45^\circ$ so that the force has different signs for $\delta = 0^\circ$ and 90° , in agreement with our predictions. As a result, the PGM moves forward and back at $\delta = 0^\circ$ and 90° , respectively. By contrast, the sign of the LOF is always positive for the OGM, though the force magnitude is sensitive to δ .

Figures 4(a) and 4(b) show the LOF calculated at different wavelengths for x and y polarization. The optical torque [38] in the z direction is also presented. The LOF phenomenon is broadband, both in magnitude and in sign. Under these linear polarization conditions, symmetry dictates that the torque must vanish. In this context, the metavehicle can drive straight forward (or backward), at the x (or y) polarization, as illustrated by insets i and ii of Fig. 1(b).

To investigate the swerving ability of the metavehicle, the force and torque were also calculated for circularly polarized plane wave incidence. The results are shown in Figs. 4(c) and 4(d). The torque is always positive for left-handed circular polarization (LCP), and negative for right-handed circular polarization (RCP). For a given wavelength, the torques induced by the LCP and RCP are of opposite signs but the same magnitude. A lateral force F_x can also be induced, but it has the same sign and magnitude for the LCP and RCP. In this regard, it should be noted that the coordinate system in our study is built based on the orientation of the metavehicle (i.e., the x axis is always in line with the long axis of the metavehicle). Therefore, the metavehicle can orbit under the action of F_x when the torque M_z is present, which realigns the metavehicle's heading, while the LOF in the y direction, F_y , is not necessary for the

orbital motion. In fact, F_y is always suppressed for the metasurface, whose geometry is symmetric about its long axis (see Note 2 of Supplement 1).

Interestingly, the sign of F_x can be changed with wavelength, in contrast to the linear polarization-induced force, whose sign is insensitive. For $F_x > 0$, the metavehicle is expected to turn left (or right) while moving forward at RCP (or LCP), a scenario depicted in inset vi (or iv) of Fig. 1(b). It is also able to turn corners while driving backward [i.e., insets iv and vi of Fig. 1(b)], occurring at $F_x < 0$ and RCP (for left turning) or LCP (for right turning). Finally, it is worth noting that, owing to the radiation pressure, the optical force in the z direction is nonzero, but it can be balanced by the gravity of the metavehicle itself in practice [21].

The presented work shows an improved LOF platform for a future metavehicle design, which provides the additional capability of reverse operation while retaining all the forward and steering elements enabled by previous designs. The metasurface is powered by a plane wave incident from beneath the metavehicle, which is then deflected on transmission through a PGM. The efficiency and range of possible deflections is increased in comparison with a conventional OGM, resulting in a wider range of strong recoil LOFs on the metavehicle. A PGM solution completes the set of 2D movements required for a general-purpose metavehicle, and the use of plane wave illumination implies that numerous metavehicles can be controlled simultaneously. Such metavehicles are therefore ideally suited for the transportation of microscopic bodies and similar applications [41–45].

As a closing remark, it is of importance to note that a comprehensive design requires a careful consideration of not only the function of the metavehicle, but also its motive force, stability, and robustness, for which one should take into account both the force and torque in each direction (see Note 3 of Supplement 1 for a detailed discussion). For example, the deflection angle of the metasurface could be increased to enhance the magnitude of the LOF. There is thus a lot of room for optimizing the PGM parameters. Such an optimization design is the subject of ongoing research.

Funding. National Natural Science Foundation of China (12274181, 11621091, 11774162, 11774164, 11804119, 11822406).

Disclosures. The authors declare no conflicts of interest.

Data availability. Data underlying the results presented in this paper are not publicly available at this time but may be obtained from the authors upon reasonable request.

Supplemental document. See Supplement 1 for supporting content.

REFERENCES

1. R. Omori, T. Kobayashi, and A. Suzuki, *Opt. Lett.* **22**, 816 (1997).
2. H. Li, Y. Cao, L.-M. Zhou, X. Xu, T. Zhu, Y. Shi, C.-W. Qiu, and W. Ding, *Adv. Opt. Photonics* **12**, 288 (2020).
3. J. L. Killian, F. Ye, and M. D. Wang, *Cell* **175**, 1445 (2018).
4. J. Millen, T. S. Monteiro, R. Pettit, and A. N. Vamivakas, *Rep. Prog. Phys.* **83**, 026401 (2020).
5. C. Gonzalez-Ballester, M. Aspelmeyer, L. Novotny, R. Quidant, and O. Romero-Isart, *Science* **374**, eabg3027 (2021).
6. Y. Liang, S. Yan, Z. Wang, R. Li, Y. Cai, M. He, B. Yao, and M. Lei, *Rep. Prog. Phys.* **83**, 032401 (2020).
7. Q. Wang, C.-H. Tu, Y.-N. Li, and H.-T. Wang, *APL Photonics* **6**, 040901 (2021).
8. J. Gieseler, J. R. Gomez-Solano, A. Magazzù, I. Pérez Castillo, L. Pérez García, M. Gironella-Torrent, X. Viader-Godoy, F. Ritort, G.

- Pesce, A. V. Arzola, K. Volke-Sepúlveda, and G. Volpe, *Adv. Opt. Photonics* **13**, 74 (2021).
9. L. Li, Z. Liu, X. Ren, S. Wang, V.-C. Su, M.-K. Chen, C. H. Chu, H. Y. Kuo, B. Liu, W. Zang, G. Guo, L. Zhang, Z. Wang, S. Zhu, and D. P. Tsai, *Science* **368**, 1487 (2020).
 10. J. Zeng, L. Li, X. Yang, and J. Gao, *Nano Lett.* **16**, 3101 (2016).
 11. J. Zeng, M. Darvishzadeh-Varcheie, M. Albooyeh, M. Rajaei, M. Kamandi, M. Veysi, E. O. Potma, F. Capolino, and H. K. Wickramasinghe, *ACS Nano* **12**, 12159 (2018).
 12. A. Arbabi, Y. Horie, M. Bagheri, and A. Faraon, *Nat. Nanotechnol.* **10**, 937 (2015).
 13. S. Wang, P. C. Wu, V.-C. Su, Y.-C. Lai, M.-K. Chen, H. Y. Kuo, B. H. Chen, Y. H. Chen, T.-T. Huang, J.-H. Wang, R.-M. Lin, C.-H. Kuan, T. Li, Z. Wang, S. Zhu, and D. P. Tsai, *Nat. Nanotechnol.* **13**, 227 (2018).
 14. T. Li, X. Li, S. Yan, X. Xu, S. Wang, B. Yao, Z. Wang, and S. Zhu, *Phys. Rev. Appl.* **15**, 014059 (2021).
 15. Y. Shi, Q. Song, I. Toftul, T. Zhu, Y. Yu, W. Zhu, D. P. Tsai, Y. Kivshar, and A. Q. Liu, *Appl. Phys. Rev.* **9**, 031303 (2022).
 16. J. J. Kingsley-Smith, M. F. Picardi, and F. J. Rodríguez-Fortuno, *Nano Lett.* **20**, 7094 (2020).
 17. K. Shen, Y. Duan, P. Ju, Z. Xu, X. Chen, L. Zhang, J. Ahn, X. Ni, and T. Li, *Optica* **8**, 1359 (2021).
 18. T. Li, X. Xu, B. Fu, S. Wang, B. Li, Z. Wang, and S. Zhu, *Photonics Res.* **9**, 1062 (2021).
 19. X. Li, Y. Zhou, S. Ge, G. Wang, S. Li, Z. Liu, X. Li, W. Zhao, B. Yao, and W. Zhang, *Opt. Lett.* **47**, 977 (2022).
 20. T. Chantakit, C. Schlickriede, B. Sain, F. Meyer, T. Weiss, N. Chattham, and T. Zentgraf, *Photonics Res.* **8**, 1435 (2020).
 21. D. Andrés, D. G. Baranov, S. Jones, G. Volpe, R. Verre, and M. Kall, *Nat. Nanotechnol.* **16**, 970 (2021).
 22. M. Nieto-Vesperinas and X. Xu, *Phys. Rev. Res.* **3**, 043080 (2021).
 23. X. Xu and M. Nieto-Vesperinas, *Phys. Rev. Lett.* **123**, 233902 (2019).
 24. J. J. Kingsley-Smith, M. F. Picardi, L. Wei, A. V. Zayats, and F. J. Rodríguez-Fortuno, *Phys. Rev. B* **99**, 235410 (2019).
 25. H. Latioui and M. G. Silveirinha, *Phys. Rev. A* **100**, 053848 (2019).
 26. J. A. Girón-Sedas, J. J. Kingsley-Smith, and F. J. Rodríguez-Fortuno, *Phys. Rev. B* **100**, 075419 (2019).
 27. S. B. Wang and C. T. Chan, *Nat. Commun.* **5**, 3307 (2014).
 28. H. Chen, H. Zheng, W. Lu, S. Liu, J. Ng, and Z. Lin, *Phys. Rev. Lett.* **125**, 073901 (2020).
 29. F. J. Rodríguez-Fortuno, N. Engheta, A. Martinez, and A. V. Zayats, *Nat. Commun.* **6**, 8799 (2015).
 30. N. K. Paul, D. Correias-Serrano, and J. S. Gomez-Diaz, *Phys. Rev. B* **99**, 121408 (2019).
 31. F. Kalhor, T. Thundat, and Z. Jacob, *Appl. Phys. Lett.* **108**, 061102 (2016).
 32. A. Hayat, J. P. Mueller, and F. Capasso, *Proc. Natl. Acad. Sci. U. S. A.* **112**, 13190 (2015).
 33. T. Zhu, Y. Shi, W. Ding, D. P. Tsai, T. Cao, A. Q. Liu, M. Nieto-Vesperinas, J. J. Saenz, P. C. Wu, and C. W. Qiu, *Phys. Rev. Lett.* **125**, 043901 (2020).
 34. Y. Shi, T. Zhu, T. Zhang, A. Mazzulla, D. P. Tsai, W. Ding, A. Q. Liu, G. Cipparrone, J. J. Saenz, and C. W. Qiu, *Light: Sci. Appl.* **9**, 62 (2020).
 35. H. Chen, Y. Jiang, N. Wang, W. Lu, S. Liu, and Z. Lin, *Opt. Lett.* **40**, 5530 (2015).
 36. M. L. Solomon, A. A. E. Saleh, L. V. Poulikakos, J. M. Abendroth, L. F. Tadesse, and J. A. Dionne, *Acc. Chem. Res.* **53**, 588 (2020).
 37. D. Ray, T. V. Raziman, C. Santschi, D. Etezadi, H. Altug, and O. J. F. Martin, *Nano Lett.* **20**, 8752 (2020).
 38. X. Xu, C. Cheng, Y. Zhang, H. Lei, and B. Li, *J. Phys. Chem. Lett.* **7**, 314 (2016).
 39. M. Nieto-Vesperinas, J. J. Sáenz, R. Gómez-Medina, and L. Chantada, *Opt. Express* **18**, 11428 (2010).
 40. M. Nieto-Vesperinas and X. Xu, *Light: Sci. Appl.* **11**, 297 (2022).
 41. F. Nan and Z. Yan, *Nano Lett.* **20**, 2778 (2020).
 42. W. Ding, T. Zhu, L.-M. Zhou, and C.-W. Qiu, *Adv. Photonics* **1**, 1 (2019).
 43. H. Zheng, X. Li, H. Chen, and Z. Lin, *Opt. Express* **29**, 42684 (2021).
 44. Y. Zhou, X. Xu, Y. Zhang, M. Li, S. Yan, M. Nieto-Vesperinas, B. Li, C.-W. Qiu, and B. Yao, *Proc. Natl. Acad. Sci. U. S. A.* **119**, e2209721119 (2022).
 45. X. Xu, Y. Yang, L. Chen, X. Chen, T. Wu, Y. Li, X. Liu, Y. Zhang, and B. Li, *Laser Photonics Rev.* **15**, 2000546 (2021).